RSC Advances

RSC Publishing

PAPER

View Article Online
View Journal | View Issue



Cite this: *RSC Advances*, 2013, **3**, 8998

# SERS-active silver nanoparticles on electrospun nanofibers facilitated *via* oxygen plasma etching

Ying Bao,[a] Chuilin Lai,[b] Zhengtao Zhu,[b] Hao Fong*[b] and Chaoyang Jiang*[a]

Received 3rd December 2012,
Accepted 28th March 2013

DOI: 10.1039/c3ra41322e

**www.rsc.org/advances**

Manipulating the interaction between inorganic building blocks and polymeric supporting materials is crucial in the fabrication and optimization of hybrid hierarchical nanostructures. Herein, oxygen plasma etching was used to modify electrospun nanofibers of poly(methyl methacrylate) (PMMA) for facilitating the growth of silver nanoparticles (Ag NPs). The PMMA nanofibers in the form of overlaid films, surface-decorated with Ag NPs, were explored as active substrates for surface-enhanced Raman scattering (SERS). Strong SERS enhancement was observed from the Ag NP–PMMA films, as well as individual nanofibers. Our work not only fabricated nanocomposite materials with controlled hierarchical structures and remarkable SERS performances, but also provided a versatile method in tuning interfacial interactions within nanostructured materials.

## Introduction

Hybrid hierarchical nanostructures provide an exciting research platform for the exploration of unique physical and chemical properties due to the integration of multifunctional building blocks within the nanostructures.[1–6] Among a variety of techniques available for the development of hybrid hierarchical nanostructures, the technique of electrospinning has attracted growing interest because of its simplicity and versatility. *Via* electrospinning, ultrathin fibers with diameters typically in the range of tens to hundreds of nanometers can be prepared.[7,8] During the last decade, the technique of electrospinning has been investigated for integrating polymers with various functional materials, such as nanoparticles,[9–12] biomolecules,[13] and luminescent ions,[14–20] and a variety of nanofibers with different morphological structures (*e.g.*, ribbon-shaped, beaded, and round-end fibers) have been reported.[21,22] Those electrospun nanostructures have been studied for various applications such as surface-enhanced Raman scattering (SERS),[10,23–25] catalysis,[26–28] antimicrobial,[29,30] tissue engineering[31–34] and drug delivery.[35]

Among assorted hybrid hierarchical nanostructures, the SERS-active electrospun nanofibers, surface-decorated and/or impregnated with metal nanoparticles, have been intensively studied because of their scalability, multifunctionality, high sensitivity, and cost-effectiveness.[36,37] SERS, as a powerful ultra-sensitive analytical technique, is capable of dramatically enhancing the Raman signals of analyte molecules adsorbed on substrates for trace level detections.[38–42] In general, there are two types of metal–polymer nanofiber that have been studied for preparing the SERS-active substrates. In type I, metal nanoparticles are embedded in the polymer nanofibers using methods such as directly electrospinning a nanoparticle-containing polymer solution,[25,43] and reducing metal ions dispersed in the polymer matrix *via* chemical reaction,[44,45] high energy irradiation,[29,46] or heat treatment.[47] For example, Zhang and co-workers electrospun a poly(vinyl alcohol) solution containing gold nanorods; the fabricated freestanding and flexible nanofibrous mats containing gold nanorods demonstrated high SERS activities.[48] The type II nanostructures have metal nanoparticles decorated on the surface of polymer nanofibers, and the fabrication methods applied in such nanomaterials include post-spinning attachment of nanomaterials,[37] seeded growth,[36] and metal sputtering coating.[49] For instance, Lee and co-workers indicated that the directed assembly of gold nanorods on highly aligned electrospun poly(2-vinyl pyridine) nanofibers would result in globally anisotropic plasmonic and SERS properties.[37] Due to the ability of direct interaction with analytes, the nanostructures prepared with the second approach would possess higher SERS performance than those prepared with the first approach. However, it is noteworthy that type II nanostructures also have some intrinsic disadvantages in considering their stability, biocompatibility, and reproducibility. Developing new methods to overcome those issues, while retaining the superior SERS activities, could be of interest to the fields of both fundamental study and practical applications.

Surface properties of polymer nanofibers play a vital role in the attachment of metal nanoparticles. These properties include surface morphology, hydrophilicity, and chemical

[a]*Department of Chemistry, University of South Dakota, 414 East Clark Street, Vermillion, SD 57069, USA. E-mail: Chaoyang.Jiang@usd.edu; Fax: 605 677 6397*
[b]*Department of Chemistry, South Dakota School of Mines and Technology, 501 East St. Joseph Street, Rapid City, SD 57701, USA. E-mail: Hao.Fong@sdsmt.edu; Fax: 605 394 1232*

functionality. Hence, surface modification is a crucial step to tune the surface chemistry of polymer nanofibers with functional groups such as $-NH_2$, –OH, and –SH. For example, Zhang and co-workers reported a surface modification method of amidoximization to produce chelating groups on polyacrylonitrile nanofibers;[50] we also prepared a SERS-active substrate *via* amidoximization of the nanofibers followed by electroless plating of silver nanoparticles.[36] These surface modifications can drastically improve the deposition of metal nanoparticles on the nanofibers. However, such surface modifications would only be suitable for limited types of polymer nanofibers. There is still a demand to identify reliable, simple, and universal methods to activate the surface of polymer nanofibers for nanoparticle attachment.

Plasma etching is a widely utilized process for surface modifications in thin film preparations and microelectronic device fabrications.[51–55] There are few studies on plasma etching for surface modification of electrospun nanofibers to prepare nanostructures. In this paper, we report the usage of oxygen plasma etching to activate the hydrophobic surface of poly(methyl methacrylate) (PMMA) nanofibers. The resulting hydrophilic surfaces were further decorated with silver nanoparticles (Ag NPs) *via* electroless plating. The final electrospun PMMA nanofibers, surface-decorated with silver nanoparticles (Ag NP–PMMA), were characterized with scanning electron microscopy (SEM), transmission electron microscopy (TEM), and confocal Raman microscopy. The Ag NP–PMMA demonstrated strong SERS enhancement, even for individual nanofibers. Our study represents an effective approach for the convenient preparation of well controlled metal nanoparticles on electrospun polymer nanofibers for SERS applications.

## Experimental

### Materials

PMMA (MW = 996 000), *N*,*N*-dimethylformamide (DMF), 1,1,2,2-tetrachloroethane (TCE), chloroform, silver nitrate ($AgNO_3$), palladium chloride ($PdCl_2$), tin chloride ($SnCl_2$), potassium hydroxide (KOH), and ammonium hydroxide ($NH_4OH$) were purchased from Sigma Aldrich (St. Louis, MO, USA). Dextrose was purchased from Fisher Scientific (Pittsburgh, PA, USA). Purified water with resistivity of 18 MΩ cm was used for the growth of silver nanoparticles.

### Preparation and modification of electrospun nanofibers

PMMA (1.4 g) was dissolved in a mixed solvent of 1.86 g DMF and 16.74 g TCE. The electrospinning setup consisted of a 20 mL plastic syringe with an 18 gauge stainless-steel needle, an electrically ground collector, and a high voltage supply (Gamma High Voltage Research Inc.). The solution was filled into the syringe and the electrospinning was carried out with a positive voltage of 20 kV applied to the stainless-steel needle. The solution feed rate of 1.5 mL $h^{-1}$ was maintained using a syringe pump (KD Scientific Inc.). PMMA nanofibers were collected on the collector covered with aluminum foil. The distance between the needle and collector was about 20 cm.

The as-electrospun PMMA nanofibrous films were treated with oxygen plasma for different periods of time, 10 s and 30 s, before the growth of silver nanoparticles. During the experiment, a sample was loaded into the vacuum chamber of a PE50 plasma system (Plasma Etch Inc.). The oxygen plasma was generated under conditions of 0.15 Torr, flow rate of 15 sccm, and 100 W RF power.

### Growth of silver nanoparticles

The growth of silver nanoparticles on the plasma-treated PMMA nanofibers was conducted *via* a two-step process using a known procedure.[36] The palladium seeding on the nanofiber surface was first carried out by a typical $SnCl_2$–$PdCl_2$ method.[56] Briefly, a plasma-treated PMMA nanofibrous film was immersed in a 3.0 mM $SnCl_2$ solution for 30 min and then in a 3.0 mM $PdCl_2$ solution for another 30 min. Thereafter, Pd seeds introduced on the surface of PMMA nanofibers were used as active sites for the following nucleation and growth of Ag NPs. Tollen's reagent (ammoniacal silver nitrate) was subsequently used for the electroless plating of Ag NPs onto the surface-activated PMMA nanofibers. A 15 M $NH_4OH$ solution was added dropwise into a 30 mL 0.1 M $AgNO_3$ solution till the brown precipitate disappeared. Then 15 mL 0.8 M KOH solution was added, which was followed by the addition of concentrated $NH_4OH$ until the solution was clear. The solution was then mixed with 3 mL 0.25 M dextrose aqueous solution and the mixture was stirred for 20 s. Finally, the activated PMMA nanofibers were immersed in the freshly prepared Tollen's reagent for electroless plating with dextrose as a reducing agent. After time periods of 15 s, 30 s, 45 s and 60 s, the resulting Ag NP decorated PMMA nanofibers were rinsed with water and dried at room temperature.

### Characterization

The morphologies of the PMMA nanofibers before and after the surface decoration of Ag NPs were examined by a Zeiss Supra 40 VP field-emission SEM. TEM images were obtained on a JEOL JEM-2100 TEM and a Technai Spirit G2 Twin (FEI Company) TEM. The SERS activities and confocal Raman maps were acquired from an Aramis confocal microscope (Horiba Jobin Yvon, Edison, NJ) equipped with diode-pumped solid-state (DPSS) lasers (532 nm). The contact angle measurements were conducted on a laboratory-made apparatus using a USB digital microscope to record the shapes of the water droplets on the nanofibrous films.

## Results and discussion

### Ag NP–PMMA nanofibrous films

The two steps for the fabrication of Ag NP–PMMA nanofibrous films are shown schematically in Fig. 1. The PMMA nanofibrous film was first treated with oxygen plasma to introduce hydroxyl groups on the surface. The treated PMMA nanofibrous films were more hydrophilic than the films prior to the treatment. The Ag NPs were then grown on the surface of the

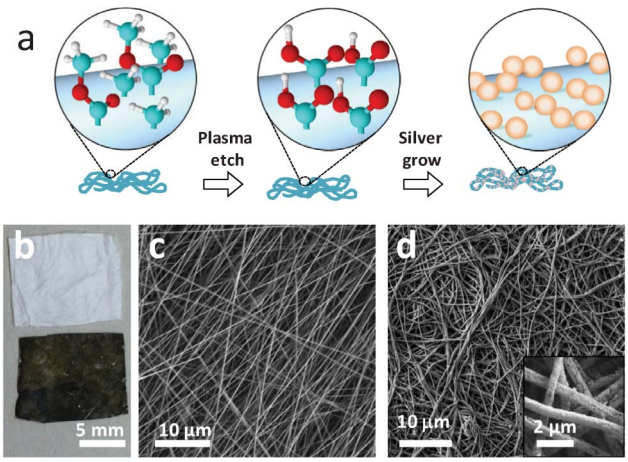


**Fig. 1** (a) Schematic showing the decoration of Ag NPs on the PMMA nanofibers; color code of the atoms: blue-carbon; red-oxygen; grey-hydrogen; (b) photograph of the PMMA film (top) and Ag NP–PMMA film (bottom); (c) and (d) SEM images of a representative PMMA nanofibrous film before and after the Ag NP decoration, respectively.

nanofibers through a known seed-mediated electroless plating method.[56] The seeding step introduced palladium seeds on the nanofiber surface, and these seeds then acted as active sites for the nucleation and growth of Ag NPs.[57] The reduction of silver ions into elemental silver using dextrose (D–CHO) is illustrated in the following equation:

$$\text{D–CHO} + 2[\text{Ag}(\text{NH}_3)_2]^+ + 3\text{OH}^- \rightarrow 2\text{Ag} + \text{D–COO}^- + 4\text{NH}_3 + 2\text{H}_2\text{O}$$

The morphology of the electrospun nanofibers is significantly influenced by the experimental parameters in the electrospinning process.[21,22,58,59] In this study, uniform PMMA nanofibers were obtained by optimizing the experimental parameters. The photograph in Fig. 1b shows the PMMA nanofibrous film before and after surface-decoration with the Ag NPs, respectively. The attachment of Ag NPs on the PMMA nanofibers changed the color of the film from white to dark brown-yellow. Further examination using SEM revealed that the PMMA film was composed of randomly overlaid nanofibers with an average diameter of 313.6 ± 42.4 nm. After the growth of Ag NPs, the morphology of the nanofibrous film changed significantly as shown in Fig. 1d; the nanofibers appeared more curved with much higher degree of conglutination as compared to those before the Ag NP attachment. Furthermore, the diameter of those nanofibers showed a slight increase that can be attributed to the deposition of the Ag NPs on the nanofiber surface. The inset of Fig. 1d is a higher magnification SEM micrograph in which aggregates of the silver nanoparticles on the surface of the PMMA nanofibers can be clearly observed. The results clearly indicated that the plasma etching process could facilitate the decoration of Ag NPs on the surface of PMMA nanofibers. With a better understanding of their process–structure–property–performance relationships, such nanofibrous films can be very useful for various applications, such as antimicrobial and SERS detections.

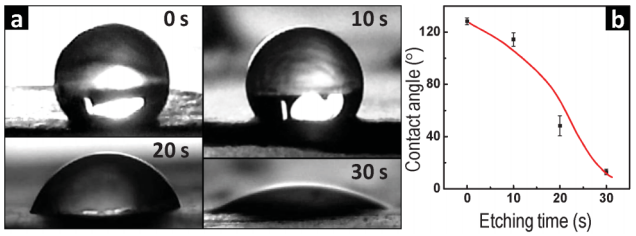


**Fig. 2** (a) Photographs of a water droplet on a plasma-treated PMMA nanofibrous film with varied etching time; (b) the change of the contact angle as a function of the etching time.

### Impact of plasma etching

In our work, the plasma etching is a key step that leads to the successful deposition of Ag NPs on the surface of the PMMA nanofibers. With the process of plasma etching, oxygen-containing functional groups can be generated on the surface of the PMMA nanofibers as evidenced by the variation of the water contact angle for the nanofibrous films (Fig. 2a). It is evident that the contact angle decreases with prolonging of the plasma etching time. Such a result indicates an increase in hydrophilicity of the PMMA nanofibrous film. The plot in Fig. 2b summarizes the values of the contact angle as a function of the plasma etching time. The untreated PMMA nanofibrous film has a large contact angle value of about 125°. With the oxygen plasma etching, the contact angle of the PMMA films has decreased, which reveals a change in the surface chemistry. The hydrophobic surface of the PMMA nanofibrous film becomes quite hydrophilic upon plasma etching for 30 s. This can be attributed to the plasma-induced oxidation of the surface methyl groups that causes the surface of the film to be more hydrophilic.[60] The resulting hydrophilic surface will facilitate the further deposition of the Ag NPs on the surface of the nanofibers.

The oxygen plasma etching plays a significant role on controlling the morphology of Ag NPs decorated on the PMMA nanofibers. To reveal the impact of plasma etching on the Ag NPs' morphology, SEM was employed to investigate the Ag NP-decorated PMMA nanofibrous films after plasma treatment for 0, 10, and 30 s, respectively (Fig. 3). In these SEM micrographs, the PMMA nanofibers become semi-transparent while the Ag NPs exhibit bright spots due to higher atomic number and stronger reflectivity to the electron beam. Fig. 3a shows the morphology of the Ag NP–PMMA nanofibers without plasma treatment (*i.e.*, the treatment time was 0 s). It is clearly seen that the Ag NPs only cover part of the nanofiber surface, while a large portion of the nanofiber surface has no Ag NPs. For the sample with 10 s oxygen plasma treatment, the coverage of the nanofibers with Ag NPs increased considerably (Fig. 3b). The Ag NPs uniformly covered the entire surface of the nanofibers when the oxygen plasma treatment time increased to 30 s. Together with the contact angle results, we can conclude that oxygen plasma etching for 30 s produced enough hydrophilic functional groups on the surface of the PMMA nanofibers for a

 

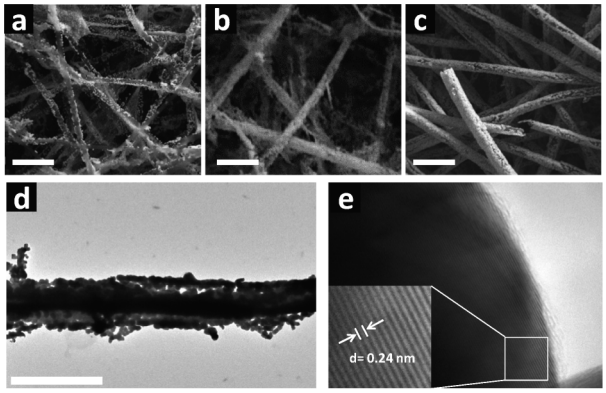


**Fig. 3** SEM images showing Ag NPs on the PMMA nanofibers (1 min growth) with varied etching times of (a) 0 s, (b) 10 s, (c) 30 s; (d) TEM image of the same sample as (c); (e) HRTEM image of a representative Ag NP showing the fringe spacing of 0.24 nm. Scale bars in all images: 2 μm.

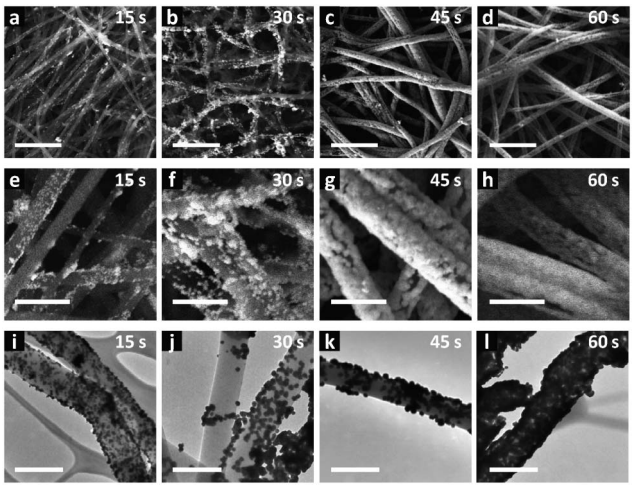


**Fig. 4** SEM (a–h) and TEM (i–l) micrographs of Ag NP–PMMA nanofibers (30 s etching) at various Ag NP growth times. Scale bars for (a–d): 4 μm; (e–h): 1 μm; and (i–l): 500 nm.

uniform decoration of the Ag NPs. It is noteworthy that some PMMA nanofibers were broken into shorter ones upon oxygen plasma treatment for 30 s (Fig. 3c), which could be due to the long process of the plasma etching and oxidation.

TEM was employed for further investigation of the Ag NPs decorated on the PMMA nanofibers. The PMMA nanofibers had smooth surfaces before the decoration with Ag NPs (image not shown). After the Ag NP-decoration, the Ag NP–PMMA fibers had rather rough surfaces due to the attachment of Ag NPs, and the nanofibrous film became dark in the TEM image (Fig. 3d). The high resolution TEM (HRTEM) micrograph of a Ag NP was obtained, in which the crystal lattice structure was clearly observed (Fig. 3e). The typical HRTEM image has crystal lattice with a spacing of 0.24 nm, which is consistent with the d-spacing of the <111> crystallographic plane of elemental silver.[61,62]

### Growth of Ag NPs

The size and density of Ag NPs on the surface of the PMMA nanofibers can be adjusted by simply changing the growth time. The growth of Ag NPs would start from the active sites on the surface of the nanofibers and then proceed toward the whole nanofiber surface. To confirm such a hypothesis, a series of Ag NP–PMMA nanofibrous films were prepared with various Ag NP growth times. The representative SEM micrographs of these films are shown in Fig. 4, for which the Ag NP growth times were 15, 30, 45, and 60 s. After 15 s, the Ag NPs emerged at some locations on the nanofiber surface, and this is attributed to the heterogeneous nucleation of elemental silver from the catalytically active Pd seeds.[57] Prolonging the growth time to 30 s resulted in more Ag NP aggregates on the PMMA nanofibers, whereas individual Ag NPs could be observed in the SEM micrograph. Such Ag NPs were larger than those with growth time of 15 s, due to the longer electroless plating process. The samples with growth times of 45 s and 60 s had numerous Ag NPs decorated on the surface of the PMMA nanofibers (Fig. 4c, 4d, 4g and 4h). These results indicate that the electroless plating of elemental silver must occur in a form of island growth on the nanofiber surface at its initial stage, and the consequent growth of Ag NPs can increase the size of the Ag NPs and thus increasing the diameter of the fibers.

TEM was used to further study the size increase of the Ag NPs when extending the growth time. The typical TEM images are shown in Fig. 4i to 4l. Aggregates of the Ag NPs were observed for all of these samples. For 15 s growth time, the average size of the Ag NPs was 30.3 ± 6.4 nm and the average diameter of the nanofibers was 318.5 ± 24.9 nm. For a growth time of 30 s, the Ag NPs had a relatively large size (55.6 ± 6.5 nm). With further prolonging of the growth time, the Ag NPs tended to grow together, making it difficult to measure the size of individual Ag NPs. The size increase of Ag NPs when extending the growth time would decrease the interparticle gaps between the Ag NPs. After 60 s growth, the Ag NPs tended to grow in all the free space around the nanofibers and thus resulting in covering the whole PMMA nanofibers (Fig. 4l). The plot of the size of Ag NPs and the diameter of the fibers as a function of the growth time is shown in Fig. 5. With the time-

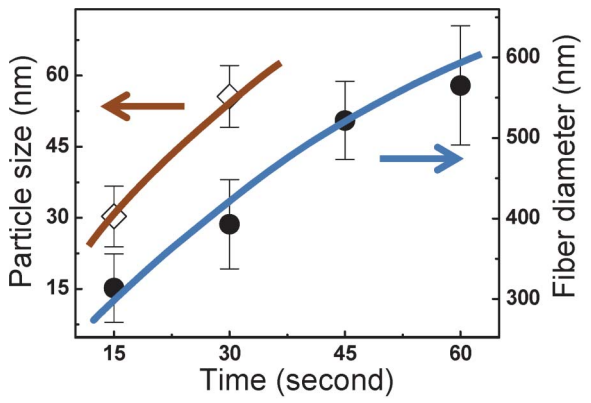


**Fig. 5** Correlations of the fiber diameter and Ag NP size with the growth time.

dependent dimension data, we are able to use reaction time to control the deposition of Ag NPs on the PMMA nanofibers.

The above results on the Ag NP deposition could be explained by a mechanism known as the Volmer–Weber mode (island growth).[63,64] Basically, the nanoparticle growth is closely related to the interaction between the nanoparticle and substrate. The island growth only occurs when the growth species are more strongly bonded with each other than to the substrate. In our work, the formation of Ag NPs was associated with the Pd seeds initially; subsequently, the growth of the Ag NPs would result in the islands due to the strong silver–silver interactions. With the increase of the growth time, the Ag NPs became larger, stacked with each other, and eventually formed a porous layer on the surface of the PMMA nanofibers.

It should be noted that non-uniform deposition of the Ag NPs was observed across the cross-section of the fibrous films. For the nanofibers inside the fibrous films, they were less etched, and the fiber surface remained hydrophobic. This would have a negative impact on the Ag NP growth. Furthermore, the reduction reaction of silver ions occurred quite fast; this could also result in less Ag NPs for the nanofibers inside the films due to the limited reagent diffusion. Nevertheless, both plasma treatment and Ag NP growth were quite uniform on the nanofiber surface. The resulting Ag NP–PMMA nanofibrous films exhibited excellent properties for their surface-sensitive applications such as SERS detection.

### SERS results

The aggregation and small interparticle gap of Ag NPs resulted in strong SERS activities for these Ag NP–PMMA nanofibrous films. 4-Mercaptobenzoic acid (4-MBA, 1 mM) was used as a probe molecule, and the typical SERS spectra are shown in Fig. 6. The main Raman peaks for 4-MBA are located at 1075 and 1590 $cm^{-1}$, which are assigned to the $\nu_{C-C}$ ring-breathing mode and stretching mode, respectively.[24,65] The SERS signals were observed in all the PMMA nanofibrous films decorated with Ag NPs. Our systematic study found that the film with Ag NP growth time of 45 s had the highest SERS intensity.

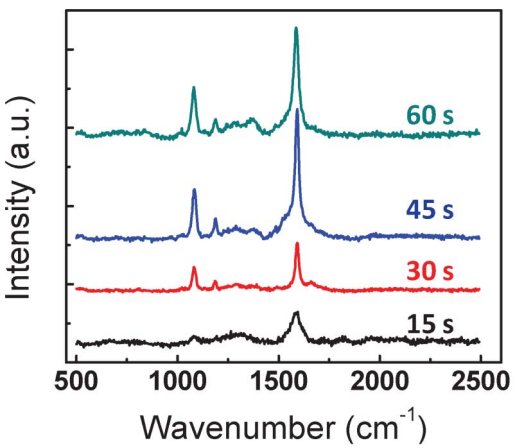


**Fig. 6** SERS spectra of 4-MBA collected on the Ag NP–PMMA nanofibrous films with varied growth time. The films were pre-treated with oxygen plasma for 30 s.

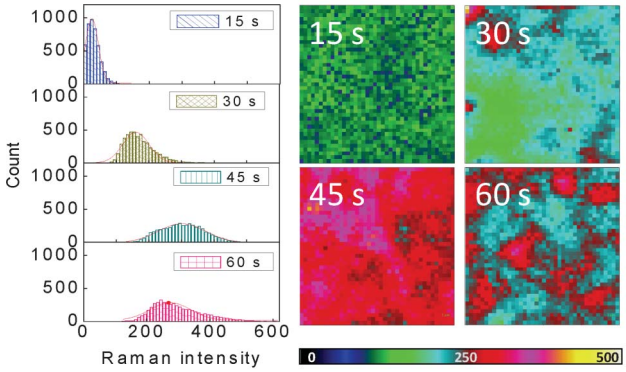


**Fig. 7** Confocal Raman mapping images for 1 mM 4-MBA molecules collected on the Ag NP–PMMA nanofibrous films with varied growth time. The films were pre-treated with oxygen plasma for 30 s. The scale bars for the Raman maps are set to be the same for easy comparison.

Confocal Raman mappings were conducted on the Ag NP–PMMA nanofibrous films with various growth times to study the uniformity of the SERS performance and to provide data for film optimization. Typical Raman maps (20 × 20 μm, 1590 $cm^{-1}$) of those films are shown in Fig. 7, together with the histograms of the intensity of the Raman signals. The mapping results depict that the Raman peak intensity was relatively uniform for all of the films. For example, the average SERS intensity for the Ag NP–PMMA nanofibrous films with 45 s growth time was 301.3 ± 72.9. The Ag NP growth time played a significant role in the SERS enhancement. Both the Raman map and intensity distribution indicated that the SERS signals increased with the growth of Ag NPs at the beginning, reached a maximum for the sample with 45 s growth time, and then slightly decreased upon further growth of Ag NPs. While the enhancement factor (EF) of SERS substrates cannot be accurately calculated due to the rough surface of the Ag NP–PMMA nanofibers, our rough estimation gave an EF value of $10^5$–$10^6$, as compared to similar Ag NP–PMMA fibrous nanostructures reported previously.[36] Similar to the results discussed above, the mapping results clearly showed that the SERS enhancement is closely related to the nanostructures of the Ag NP aggregates on the PMMA nanofibers.[36,66] In the initial growth stage, Ag NPs were far apart from each other, which would not generate effective Raman hot spots. With the size increase of the Ag NPs, the interparticle gap was reduced, resulting in the formation of Raman hot spots. With further growth of the Ag NPs, however, the de-generation of Raman hot spots occurred due to the closing-up of the interparticle gaps.

The distribution of Raman hot spots can be "visualized" with confocal Raman mapping of individual Ag NP–PMMA nanofibers. The location and shape of the Ag NP–PMMA nanofibers can be observed under an optical microscope. Fig. 8a shows several curved individual Ag NP–PMMA nanofibers on a glass substrate. The same area was investigated with the confocal Raman technique, and the SERS map is shown in Fig. 8b. The strong SERS signals were obtained from the locations of the nanofibers (which were decorated with Ag NPs). The Raman map shows a similar pattern to the

 

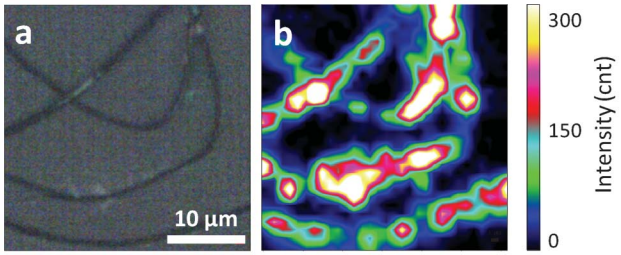


**Fig. 8** (a) Optical image of several individual Ag NP–PMMA nanofibers; (b) confocal Raman image of the same area.



optical image, indicating the effective SERS enhancement of Ag NPs on the nanofibers. In other words, such a Raman map identified the location and the density of the Raman hot spots, which were generated by the Ag NP aggregations on the nanofibers. It is very intriguing to observe the strong SERS signals from individual nanofibers, which is valuable in both the fundamental study of SERS-active substrates and potential applications such as optics, electronic, and sensing technology.

Compared with two dimensional SERS substrates, such three dimensional SERS substrates have recently received more attention due to their highly porous structure and great potential for superior SERS performance. As we know, the 3D nanostructures are ideal substrates for efficient light interaction, they have large surface area for molecular adsorption, and are capable of having a large density of Raman hot spots.[67] Examples of 3D SERS substrates can be found in the recent literature.[68–71] Our work can be included in that field of study, and has clearly demonstrated a novel approach in fabricating 3D SERS substrates. With a better understanding on the structure–property relationship of the silver nanoparticles in the nanocomposites, we can conduct further structural optimization and thus develop novel SERS substrates with much better reproducibility, stability, and sensitivity.

## Conclusion

In summary, a facile method to fabricate the hybrid hierarchical nanostructures of Ag NPs decorated on the surface of electrospun PMMA nanofibers has been explored, and the resulting Ag NP–PMMA nanofibrous film demonstrated strong SERS activities. The oxygen plasma etching is effective in increasing the hydrophilicity of the PMMA nanofibers and thus in facilitating the growth of the Ag NPs. The SERS performance has been studied from Ag NP–PMMA nanofibrous films as well as individual nanofibers. This study has demonstrated a successful approach to prepare hybrid hierarchical SERS substrates with controlled morphologies, structures, and properties for broad applications.

## Acknowledgements

This research was supported by the NSF (award numbers: EPS-0903804 and DGE-0903685), the NASA (Cooperative Agreement Number: NNX10AN34A), and the State of South Dakota. Some TEM studies were conducted on the instrument funded by the NSF (award number: CHE-0840507). The authors are grateful to Drs. James Hoefelmeyer, Edward Duke, and Phil Ahrenkiel, for helping with the electron microscopic characterizations.

## References

1 S. Shukla, K.-T. Kim, A. Baev, Y. K. Yoon, N. M. Litchinitser and P. N. Prasad, *ACS Nano*, 2010, **4**, 2249–2255.
2 X. Lu, Y. Zhao, C. Wang and Y. Wei, *Macromol. Rapid Commun.*, 2005, **26**, 1325–1329.
3 K. Yin, L. Zhang, C. Lai, L. Zhong, S. Smith, H. Fong and Z. Zhu, *J. Mater. Chem.*, 2011, **21**, 444–448.
4 Y. Bao, Q. A. N. Luu, Y. Zhao, H. Fong, P. S. May and C. Jiang, *Nanoscale*, 2012, **4**, 7369–7375.
5 D. Li, A. Babel, S. A. Jenekhe and Y. Xia, *Adv. Mater.*, 2004, **16**, 2062–2066.
6 Y. Bao, Q. A. N. Luu, C. Lin, J. M. Schloss, P. S. May and C. Jiang, *J. Mater. Chem.*, 2010, **20**, 8356–8361.
7 D. Li and Y. Xia, *Adv. Mater.*, 2004, **16**, 1151–1170.
8 T. Han, D. H. Reneker and A. L. Yarin, *Polymer*, 2007, **48**, 6064–6076.
9 L. Balan, M. Jin, J.-P. Malval, H. Chaumeil, A. Defoin and L. Vidal, *Macromolecules*, 2008, **41**, 9359–9365.
10 Y. Wang, Y. Li, S. Yang, G. Zhang, D. An, C. Wang, Q. Yang, X. Chen, X. Jing and Y. Wei, *Nanotechnology*, 2006, **17**, 3304.
11 H. Kong and J. Jang, *Biomacromolecules*, 2008, **9**, 2677–2681.
12 Q. B. Yang, D. M. Li, Y. L. Hong, Z. Y. Li, C. Wang, S. L. Qiu and Y. Wei, *Synth. Met.*, 2003, **137**, 973–974.
13 E. H. Sanders, R. Kloefkorn, G. L. Bowlin, D. G. Simpson and G. E. Wnek, *Macromolecules*, 2003, **36**, 3803–3805.
14 J. Wu and J. L. Coffer, *Chem. Mater.*, 2007, **19**, 6266–6276.
15 L. Xu, H. Song, B. Dong, Y. Wang, X. Bai, G. Wang and Q. Liu, *J. Phys. Chem. C*, 2009, **113**, 9609–9615.
16 S. Tan, X. Feng, B. Zhao, Y. Zou and X. Huang, *Mater. Lett.*, 2008, **62**, 2419–2421.
17 S. S. Tang, C. L. Shao and S. Z. Li, *Chin. Chem. Lett.*, 2007, **18**, 465–468.
18 G. Dong, Y. Chi, X. Xiao, X. Liu, B. Qian, Z. Ma, E. Wu, H. Zeng, D. Chen and J. Qiu, *Opt. Express*, 2009, **17**, 22514–22519.
19 H. Song, H. Yu, G. Pan, X. Bai, B. Dong, X. T. Zhang and S. K. Hark, *Chem. Mater.*, 2008, **20**, 4762–4767.
20 G. Dong, X. Xiao, Y. Chi, B. Qian, X. Liu, Z. Ma, E. Wu, H. Zeng, D. Chen and J. Qiu, *J. Mater. Chem.*, 2010, **20**, 1587–1593.
21 S. Koombhongse, W. Liu and D. H. Reneker, *J. Polym. Sci., Part B: Polym. Phys.*, 2001, **39**, 2598–2606.
22 L. H. C. Mattoso, R. D. Offeman, D. F. Wood, W. J. Orts and E. S. Medeiros, *Can. J. Chem.*, 2008, **86**, 590–599.
23 Y. Wang, Q. Yang, G. Shan, C. Wang, J. Du, S. Wang, Y. Li, X. Chen, X. Jing and Y. Wei, *Mater. Lett.*, 2005, **59**, 3046–3049.
24 D. He, B. Hu, Q.-F. Yao, K. Wang and S.-H. Yu, *ACS Nano*, 2009, **3**, 3993–4002.
25 C.-L. Zhang, K.-P. Lv, H.-P. Cong and S.-H. Yu, *Small*, 2012, **8**, 648–653.

26 H. Kang, Y. Zhu, X. Yang, Y. Jing, A. Lengalova and C. Li, *J. Colloid Interface Sci.*, 2010, **341**, 303–310.
27 Y. Dai, W. Liu, E. Formo, Y. Sun and Y. Xia, *Polym. Adv. Technol.*, 2011, **22**, 326–338.
28 A. M. Bazargan, S. Ghashghai, M. Keyanpour-rad and M. E. Ganji, *RSC Adv.*, 2012, **2**, 1842–1845.
29 J. Song, H. Kang, C. Lee, S. H. Hwang and J. Jang, *ACS Appl. Mater. Interfaces*, 2011, **4**, 460–465.
30 A. Niu, Y. Han, J. Wu, N. Yu and Q. Xu, *J. Phys. Chem. C*, 2010, **114**, 12728–12735.
31 J. Xie, M. R. MacEwan, A. G. Schwartz and Y. Xia, *Nanoscale*, 2010, **2**, 35–44.
32 W. Cui, Y. Zhou and J. Chang, *Sci. Technol. Adv. Mater.*, 2010, **11**, 014108.
33 N. Ashammakhi, A. Ndreu, L. Nikkola, I. Wimpenny and Y. Yang, *Regener. Med.*, 2008, **3**, 547–574.
34 J. Lannutti, D. Reneker, T. Ma, D. Tomasko and D. Farson, *Mater. Sci. Eng., C*, 2007, **27**, 504–509.
35 Z. Hou, C. Li, P. Ma, G. Li, Z. Cheng, C. Peng, D. Yang, P. Yang and J. Lin, *Adv. Funct. Mater.*, 2011, **21**, 2356–2365.
36 L. Zhang, X. Gong, Y. Bao, Y. Zhao, M. Xi, C. Jiang and H. Fong, *Langmuir*, 2012, **28**, 14433–14440.
37 C. H. Lee, L. Tian, A. Abbas, R. Kattumenu and S. Singamaneni, *Nanotechnology*, 2011, **22**, 275311.
38 S. L. Kleinman, R. R. Frontiera, A.-I. Henry, J. A. Dieringer and R. P. Van Duyne, *Phys. Chem. Chem. Phys.*, 2013, **15**, 21–36.
39 X. Gong, Y. Bao, C. Qiu and C. Jiang, *Chem. Commun.*, 2012, **48**, 7003–7018.
40 Y. Bao, L. Vigderman, E. R. Zubarev and C. Y. Jiang, *Langmuir*, 2012, **28**, 923–930.
41 A. Tao, F. Kim, C. Hess, J. Goldberger, R. He, Y. Sun, Y. Xia and P. Yang, *Nano Lett.*, 2003, **3**, 1229–1233.
42 N. A. A. Hatab, J. M. Oran and M. J. Sepaniak, *ACS Nano*, 2008, **2**, 377–385.
43 J. Han, L. Li and R. Guo, *Macromolecules*, 2010, **43**, 10636–10644.
44 E. Han, D. Wu, S. Qi, G. Tian, H. Niu, G. Shang, X. Yan and X. Yang, *ACS Appl. Mater. Interfaces*, 2012, **4**, 2583–2590.
45 J. Bai, Y. Li, M. Li, S. Wang, C. Zhang and Q. Yang, *Appl. Surf. Sci.*, 2008, **254**, 4520–4523.
46 A. Akhavan, N. Sheikh and R. Beteshobabrud, *J. Nucl. Sci. Technol.*, 2010, **50**, 80–84.
47 H.-S. Park, H.-S. Park and M.-S. Gong, *Macromol. Res.*, 2010, **18**, 897–903.
48 H. Zhang, D. Xu, Y. Huang and X. Duan, *Chem. Commun.*, 2011, **47**, 979–981.
49 H. He, W. Cai, Y. Lin and Z. Dai, *Langmuir*, 2010, **27**, 1551–1555.
50 C. Zhang, Q. Yang, N. Zhan, L. Sun, H. Wang, Y. Song and Y. Li, *Colloids Surf., A*, 2010, **362**, 58–64.
51 S. Tang, N. Lu, J. K. Wang, S.-K. Ryu and H.-S. Choi, *J. Phys. Chem. C*, 2007, **111**, 1820–1829.
52 C. M. Chan, T. M. Ko and H. Hiraoka, *Surf. Sci. Rep.*, 1996, **24**, 1–54.
53 B. T. Ginn and O. Steinbock, *Langmuir*, 2003, **19**, 8117–8118.
54 S. Zhang, H. Niu, Y. Lan, C. Cheng, J. Xu and X. Wang, *J. Phys. Chem. C*, 2011, **115**, 22025–22034.
55 X.-Y. Yu, T. Luo, Y.-X. Zhang, Y. Jia, B.-J. Zhu, X.-C. Fu, J.-H. Liu and X.-J. Huang, *ACS Appl. Mater. Interfaces*, 2011, **3**, 2585–2593.
56 L. Bortolotto, *Direct hydroxylation of benzene to phenol in a microstructured Pd-Based membrane reactor*, KIT Scientific Publishing, Karlsruhe, Germany, 2011.
57 F. Ochanda and W. E. Jones, *Langmuir*, 2005, **21**, 10791–10796.
58 S. L. Shenoy, W. D. Bates, H. L. Frisch and G. E. Wnek, *Polymer*, 2005, **46**, 3372–3384.
59 J. Shui and J. C. M. Li, *Nano Lett.*, 2009, **9**, 1307–1314.
60 M.-H. Lin, C.-F. Chen, H.-W. Shiu, C.-H. Chen and S. Gwo, *J. Am. Chem. Soc.*, 2009, **131**, 10984–10991.
61 C.-H. Hsia, M.-Y. Yen, C.-C. Lin, H.-T. Chiu and C.-Y. Lee, *J. Am. Chem. Soc.*, 2003, **125**, 9940–9941.
62 B. Wang, G. T. Fei, Y. Zhou, B. Wu, X. Zhu and L. Zhang, *Cryst. Growth Des.*, 2008, **8**, 3073–3076.
63 G. Cao, *Nanostructures & nanomaterials : synthesis, properties & applications*, Imperial College Press, London, Hackensack, NJ, 2004.
64 J. Yang, T. Wang, H. Wang, F. Zhu, G. Li and D. Yan, *J. Phys. Chem. B*, 2008, **112**, 7821–7825.
65 M. Zhang, A. Zhao, D. Li, H. Sun, D. Wang, H. Guo, Q. Gao, Z. Gan and W. Tao, *Analyst*, 2012, **137**, 4584–4592.
66 C. Farcau and S. Astilean, *J. Phys. Chem. C*, 2010, **114**, 11717–11722.
67 H. Ko, S. Singamaneni and V. V. Tsukruk, *Small*, 2008, **4**, 1576–1599.
68 R. Kodiyath, T. A. Papadopoulos, J. Wang, Z. A. Combs, H. Li, R. J. C. Brown, J. L. Bredas and V. V. Tsukruk, *J. Phys. Chem. C*, 2012, **116**, 13917–13927.
69 P. Xu, N. H. Mack, S. H. Jeon, S. K. Doorn, X. J. Han and H. L. Wang, *Langmuir*, 2010, **26**, 8882–8886.
70 Y. H. Ngo, D. Li, G. P. Simon and G. Garnier, *Langmuir*, 2012, **28**, 8782–8790.
71 C. H. Lee, M. E. Hankus, L. Tian, P. M. Pellegrino and S. Singamaneni, *Anal. Chem.*, 2011, **83**, 8953–8958.

 